NANO LETTERS

pubs.acs.org/NanoLett Letter

Damage-Tolerant Wood Layers for Corrosion Protection of Metal Structures

Sicen Yu, Yu Liu, Qiongyu Chen, Xiaolu Yu, Gayea Hyun, Shen Wang, Yuhang Ye, Jiaqi Feng, Zheng Chen, Feng Jiang, Joseph King, Teng Li,* Liangbing Hu,* and Ping Liu*

Cite This: *Nano Lett.* 2024, 24, 245−253 Read Online

ACCESS | Metrics & More | Article Recommendations | Supporting Information

ABSTRACT: Mechanically strong and damage-tolerant corrosion protection layers are of great technological importance. However, corrosion protection layers with high modulus (>1.5 GPa) and tensile strength (>100 MPa) are rare. Here, we report that a 130 μm thick densified wood veneer with a Young's modulus of 34.49 GPa and tensile strength of 693 MPa exhibits both low diffusivity for metal ions and the ability of self-recovery from mechanical damage. Densified wood veneer is employed as an intermediate layer to render a mechanically strong corrosion protection structure, referred to as "wood corrosion protection structure", or WCPS. The corrosion rate of low-carbon steel protected by WCPS is reduced by 2 orders of magnitude than state-of-the-art corrosion protection layers during a salt spray test. The introduction of engineered wood veneer as a thin and mechanically strong material points to new directions of sustainable corrosion protection design.

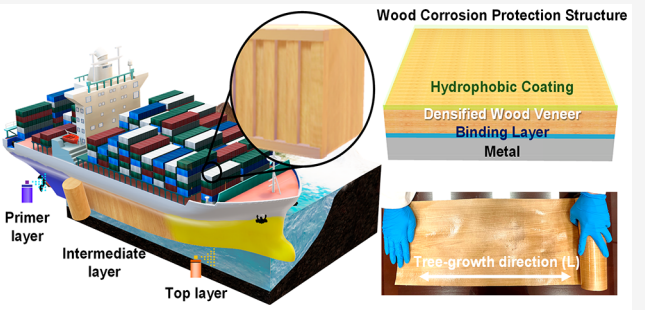

KEYWORDS: *corrosion protection, engineered wood, intermediate layer, mechanical strength, blister formation*

Protective layers are ubiquitous in life.[1] They protect the underlying materials from harsh and corrosive environments in different fields ranging from automobiles, buildings, to military equipment, particularly those exposed to a high concentrations of salts.[2−5] Defect-free protective layers have a lifespan of up to 20 years; however, layer damage is inevitable when exposed to harsh environments.[6,7] In the case of corrosion protection, even small, local defects can trigger a cascade of subsequent adverse reactions of corrosion propagation and ultimately catastrophic structural failure within a short period of time.[8,9] For this reason, enhancing the damage tolerance of protective layers is highly desired.

To mitigate the impact of local damage, self-healing layers or agents have been widely reported, which enable damage closure and healing to recover their original properties via intrinsic and/or extrinsic mechanisms.[10−12] Most intrinsic healing approaches are based on reversible physical or chemical bond formation, such as disulfide bond reshuffling. The resulting layer usually suffers from low mechanical strength.[13] Among extrinsic healing approaches, employing epoxy-based healing agents is a popular strategy.[14] Healing agents are stored in capsules embedded in the coating layer that can be released in response to specific environmental changes such as exposure to air due to crack formation.[15,16] Alternatively, introducing chromium(VI) compounds in the coating layer used to be widely used for corrosion protection.[17,18] These compounds can form dense passivating layers on freshly exposed metal surfaces. Unfortunately, chromium(VI) is a highly carcinogenic substance and has been banned by many countries.[19] It is worth noting that the effectiveness of the self-healing processes based on extrinsic approaches is highly dependent on the amount of healing agents in the protective layer since they are consumptive.[20] Furthermore, many healing agents are hydrophilic and will trigger osmotic driven water transport through the protective layer.[8,21] Effendy et al. showed that the local blisters would trigger a global failure, such as complete delamination and breakage of the protective layer if the osmotic pressure exceeds the elastic limit of the protective layer.[8] The formation of "blisters" due to this mechanism and the resultant coating failure remain a significant challenge.[8,22,23] An alternative strategy to improve the durability of protective layers is to use layers with inherently high mechanical strength.[24−26] Chuang et al. reports that the rate of cathodic blister formation under stiff coatings (Young's modulus of 1 GPa) is 3 orders of magnitude lower than soft coatings (Young's modulus of 0.01 GPa).[27] However, thin, structurally stable layers with high

Received: October 9, 2023
Revised: December 22, 2023
Accepted: December 26, 2023
Published: December 29, 2023

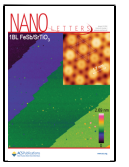

https://doi.org/10.1021/acs.nanolett.3c03856
Nano Lett. 2024, 24, 245−253

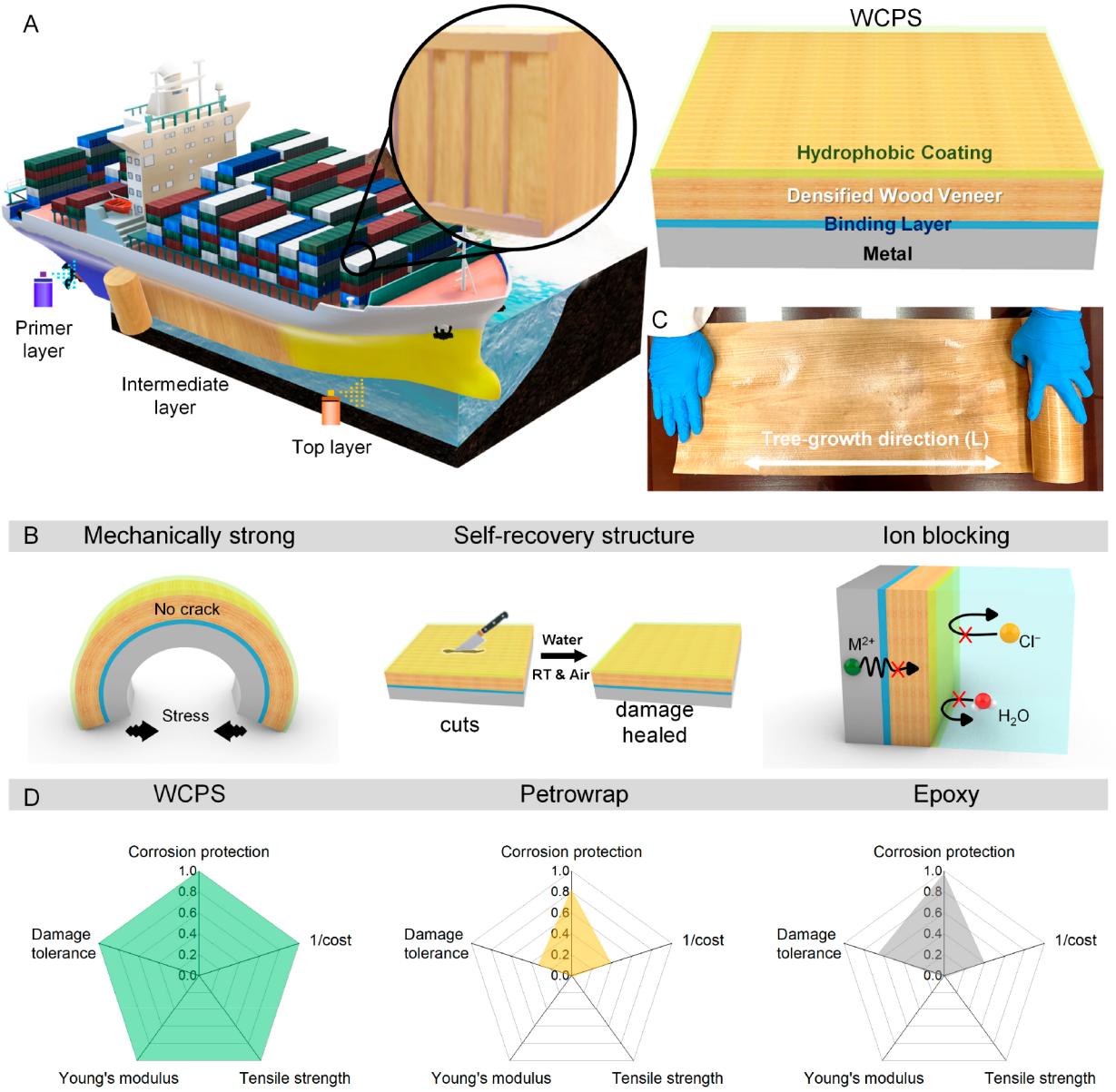

Figure 1. Structural wood layer for corrosion protection. (A, B) Schematic diagram of WCPS consisted of a densified wood veneer intermediate layer that is bonded with the metal substrate on one side and protected with a hydrophobic layer on the other. WCPS is thin (~200 μm thick), mechanically strong (347 MPa in strength and 16 GPa in Young's modulus), self-recoverable when damaged, and capable of substantially blocking ion transport for durable, fault-tolerant corrosion protection. (C) Photograph of densified wood veneer. (D) Performance comparison of WCPS, petrowrap, and epoxy (Tables S4 and S5).

damage resistance are rare.[28−30] The Young's modulus and tensile strength of most protective layers are less than 1.5 GPa and 100 MPa, respectively (Table S1). Hence, developing a self-recoverable thin material coupled with mechanically strong properties is critical to developing durable corrosion protection layers.

Densified wood is an emerging class of engineered wood material that is light, sustainable, scalable, and low-corrosivity.[31−33] Cellulose-based materials have been reported for exhibiting some degree of self-healing ability.[34,35] Here, we report a thin densified wood layer, termed a densified wood veneer, that is mechanically strong, highly resistant to mechanical damage, and capable of self-recovery triggered by exposure to water (Figure 1). Further, the layer greatly reduces ion transport. These traits make the wood veneer a promising component for corrosion protection layers. A protective structure for highly corrosive marine environments usually consists of a primer, one or several intermediate layers, and a topcoat.[36,37] The primer provides adhesion to the metal substrate, the top coat mitigates the effect of ultraviolet and water, and the intermediate layer provides the main protective functions, including blocking of water and ion transport and maintenance of the structural integrity of the coating system.[38,39] Here, we build a wood-based three-layer system (WCPS, Figure 1): an epoxy binding layer as the primer, a densified wood veneer as the intermediate layer, and a hydrophobic layer as the topcoat. We have found that introducing a mechanically strong intermediate layer transforms the structural stability of the coating structure and its durability as a corrosion protection layer. Our findings point to a new strategy for the design of corrosion protection layers. Instead of using hazardous corrosion inhibitors and self-healing

https://doi.org/10.1021/acs.nanolett.3c03856
Nano Lett. 2024, 24, 245−253

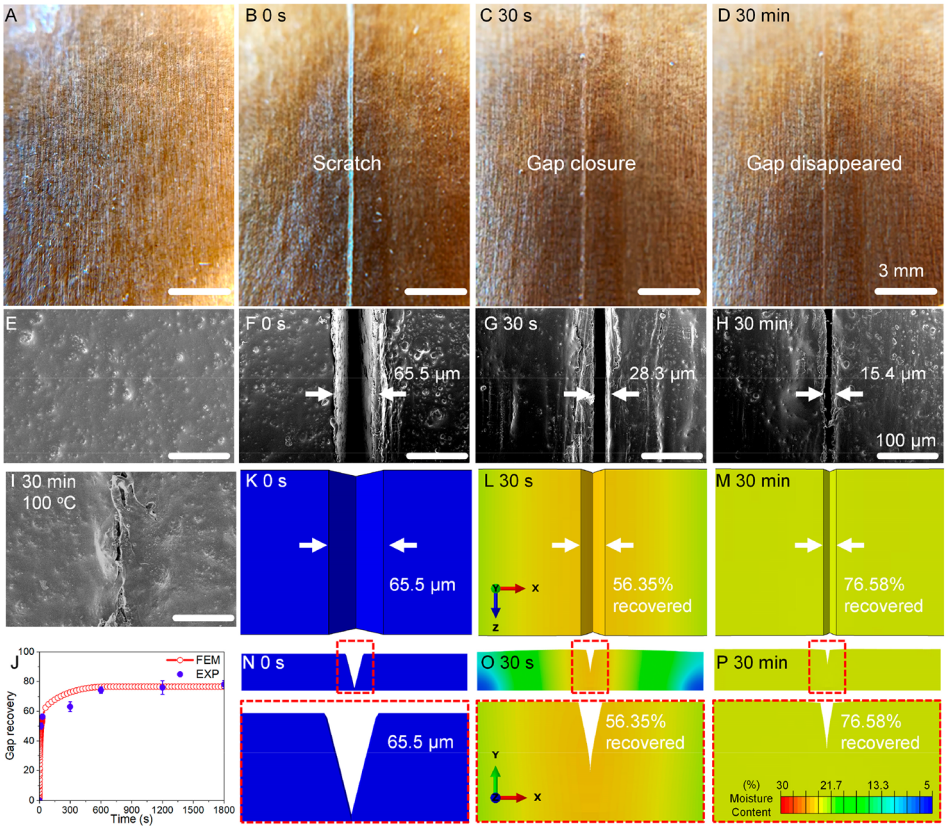

Figure 2. Self-recovery of a densified wood veneer upon mechanical damage. The self-recovering process of densified wood veneer was evaluated by (A–D) digital images and (E–H) SEM at room temperature. (I) SEM of self-recovered densified wood with hot pressing (30 min, 100 °C and 1 kPa). The scale bars in (A–D) are 3 mm and in (E–I) are 100 μm, respectively. (J) FEM simulated and measured gap recovery rate as a function of the elapsed time at room temperature. The error bars describe the distribution of three repeated data points from experiment. Simulated contour plots of moisture content on (K–M) the tangential-longitudinal plane and (N–P) the radial-transverse plane of densified wood veneer around the scratch at t = 0, 30, and 30 min, respectively, upon adding water. Red-dashed blocks are the zoomed-in views around the center-notched regions.

agents to maintain the corrosion protection function, our work shows that introducing a sustainable, damage-tolerant, and structurally strong intermediate layer is an efficient approach to minimize metal corrosion.

We employ a three-step approach for the fabrication of densified wood veneer by a chemical treatment of natural wood followed by hot-pressing[31] and finally finished with a hydrophobic coating. Chemical treatment selectively removes hemicelluloses and lignin, making wood a low-corrosivity material to metal (Figure S1).[33] Densified wood veneer has a uniform thickness of 130 μm with long and highly aligned cellulose fibers (Figure 2A). Analysis by cryo-focused ion beam (cryo-FIB) and scanning electron microscopy (SEM) shows the structure is highly dense with no obvious porosity (Figure 3G,H). The dense structure will enhance the interaction among wood fibers that is responsible for its mechanical strength.[31] Specifically, densified wood veneer exhibits a Young's modulus of 34.5 GPa and a tensile strength of 693 MPa in the direction along the cellulose fibers, which is 2 orders of magnitude higher than state-of-the-art (SOA) corrosion protection layers (petrowrap and epoxy, Figure S2). The corresponding values are 2.23 GPa and 22.43 MPa in the direction perpendicular to cellulose fibers (Figure S3). Petrowrap is a commercial material made of fibers embedded in slack wax, microcrystalline wax, and talc (Figure S4A). It is widely used to protect substrates exposed to seawater and salt air.[40] The "Epoxy" coating is a marine-grade epoxy ordered from TotalBoat (Figure S4B). We have evaluated the resistance to mechanical damage (chipping, scribing, and bending; see Methods) of densified wood veneer and SOA corrosion protection layers (Figure S5 and Movies S1, S2, S3, and S4). Petrowrap contains fiber frameworks with good flexibility to accommodate bending but itself is soft leading to a poor resistance to chipping and scribing. Epoxy is dense and strong but brittle; hence, it is resistant to chipping but vulnerable to bending and scribing. In contrast, densified wood veneer, characterized by both fiber frameworks and a highly dense structure, offers an exceptional combination of flexibility and a notable Brinell hardness number of 37 ± 5.20 (Figure S6). Remarkably, it showed no cracks after chipping and bending tests under an optical microscope. After the scribing test, no indentation can be found on the underlying metal surface as shown by SEM (Figure S4C and Figure S7), except when scribing is applied parallel to the wood-growth direction. However, this issue can be mitigated by its self-recovery ability, as discussed below. Hence, introducing densified wood veneer as an intermediate layer can enhance the structural stability of the whole protective structure and maintain its corrosion protection function under harsh conditions.

Mechanical damage due to external forces is inevitable during the service life of the corrosion protection layers. In this regard, it will be highly desirable for the protective layer to exhibit a self-recovery ability. In this work, the term of "self-recovery" is used to describe its ability to mostly recover the

https://doi.org/10.1021/acs.nanolett.3c03856
Nano Lett. 2024, 24, 245–253

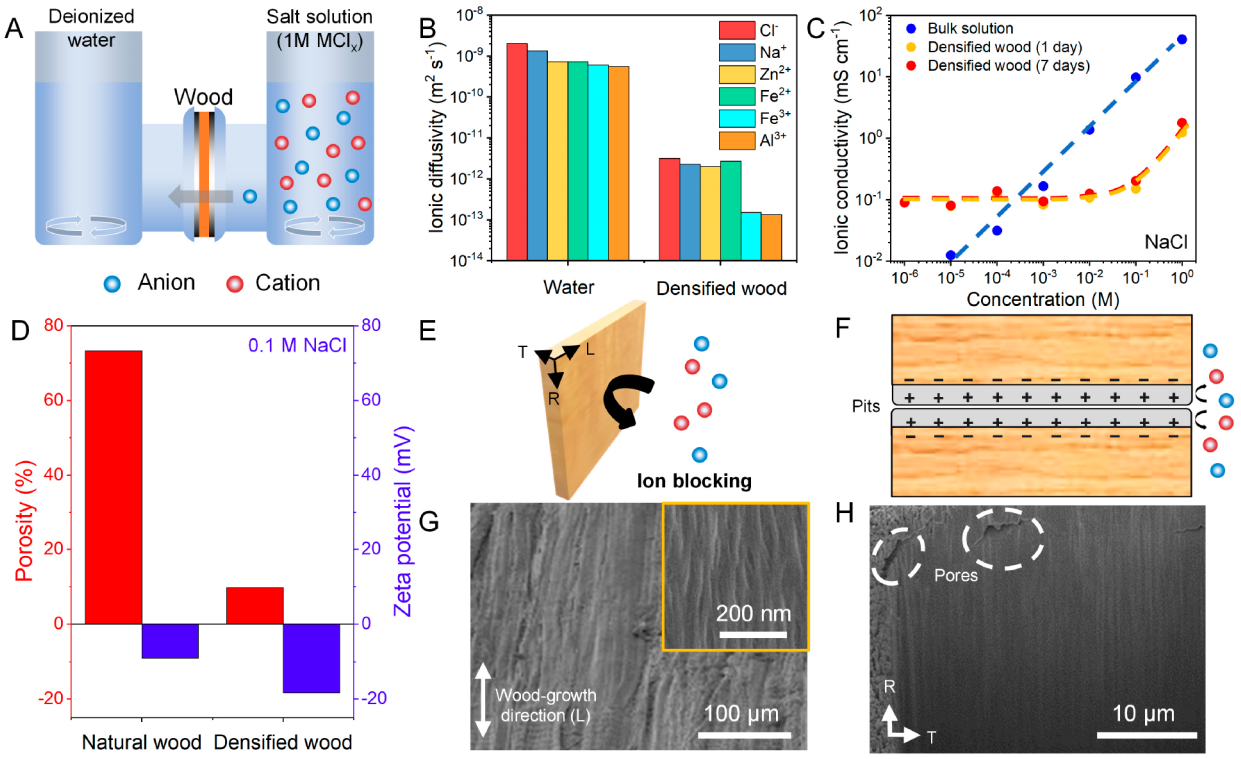

Figure 3. Ion blocking in densified wood veneer. (A) Schematic diagram of the H-cell for concentration-driven dialysis diffusion measurement. (B) Diffusivities of Cl^-, Na^+, Zn^{2+}, Fe^{2+}, Fe^{3+}, and Al^{3+} in bare densified wood veneer and in water. (C) Ionic conductivity of the densified wood veneer and deionized water when equilibrated with various NaCl concentrations. (D) Porosities and zeta potentials of natural basswood and densified wood. Schematic illustration of (E) ion blocking function of densified wood veneer and (F) the mechanism of Donnan exclusion. (G) SEM image of the densified wood veneer (without hydrophobic coating). (Inset) SEM image of the nanoscale-aligned cellulose fibers of the densified wood veneer. (H) Cryo-focused ion beam SEM image of the densified wood veneer perpendicular to the L direction, clearly showing the dense structure with few pores in the RT plane.

shape after surface damage as well as the ability to retain most of its mechanical strength. We evaluated the performance of densified wood veneer by scratching the wood surface along the direction of the wood growth, which is most likely to cause damage, followed by contacting it with water (Movie S5). Scratching on the densified wood veneer results in a 65.5 μm gap between the wood fibers (Figure 2B,F). After contacting with water, the gap decreases to 28.3 μm in the first 30 s (recovery ratio: 56.8%, Figure 2C,G) and 15.4 μm in the first 30 min (recovery ratio: 76.5%, Figure 2D,H). To evaluate the effect of hot pressing on structural recovery, we use a clothes iron as a heat source (100 °C) to assist the self-recovery behavior of densified wood veneer in contact with water. The pressure of pressing is only due to the weight of the clothes iron itself (about 1 kPa). As a result, the gap created by scratching is almost closed within 30 min (Figure 2I). Hence, densified wood veneer exhibits some self-recovery ability, which can be further enhanced when combined with hot pressing. In addition, we evaluate the influence of increasing water content due to the uptake through the damaged area on the mechanical strength of densified wood veneer (Figure S8). The wood veneer exhibits a tensile strength/Young's modulus of 517 MPa/23.2 GPa, which are still 2 orders of magnitude higher than SOA corrosion protection layers (Figure S2). This indicates the effective moisture resistance of the WCPS. Additional optimization in coating materials has the potential to further enhance the overall stability. The self-recovery property is based on the dry-swollen cycle of wood fibers. Since the water will be retained in the structure, further repair based on this mechanism will be much less effective in the rare occasion that further damage occurs at the same location. In addition, while it is very resistant to scratches perpendicular to the fiber direction, its self-recovery ability is somewhat diminished. Enhancing the self-recovery ability in the perpendicular direction is also an important topic for additional study.

To unveil the mechanism of the self-recovery of densified wood veneer, we use finite element modeling (FEM) to simulate the recovery process by considering the coupled water diffusion and mechanical deformation in densified wood veneer (see Methods). It is evident that during the first 30 s, the dry densified wood veneer absorbs water instantly and swells rapidly upon the addition of water, leading to a significant gap recovery of 56.4% (Figure 2J). After the first 30 s, the densified wood veneer continues to absorb water near the gap but in a rather slow manner due to the significantly reduced gradient of moisture content in the wood veneer. After 30 min, the water absorption by the densified wood veneer approaches an equilibrium state, leading to a gap recovery rate of 76.6%. Figure 2 panels K–P show the snapshots of the simulation results at 0 s, 30 s, and 30 min of water absorption in the top view and side view, respectively, compared with the experimental images at the same instants. The color shades in Figure 2K–P plot the moisture content in densified wood veneer near the scratch in the top and side view, respectively. The moisture content around the scratch in the densified wood veneer is 5% initially, then spikes to nearly 26% within the first 30 s, and gradually equilibrates to ~23% after 30 min of water

https://doi.org/10.1021/acs.nanolett.3c03856
Nano Lett. 2024, 24, 245–253

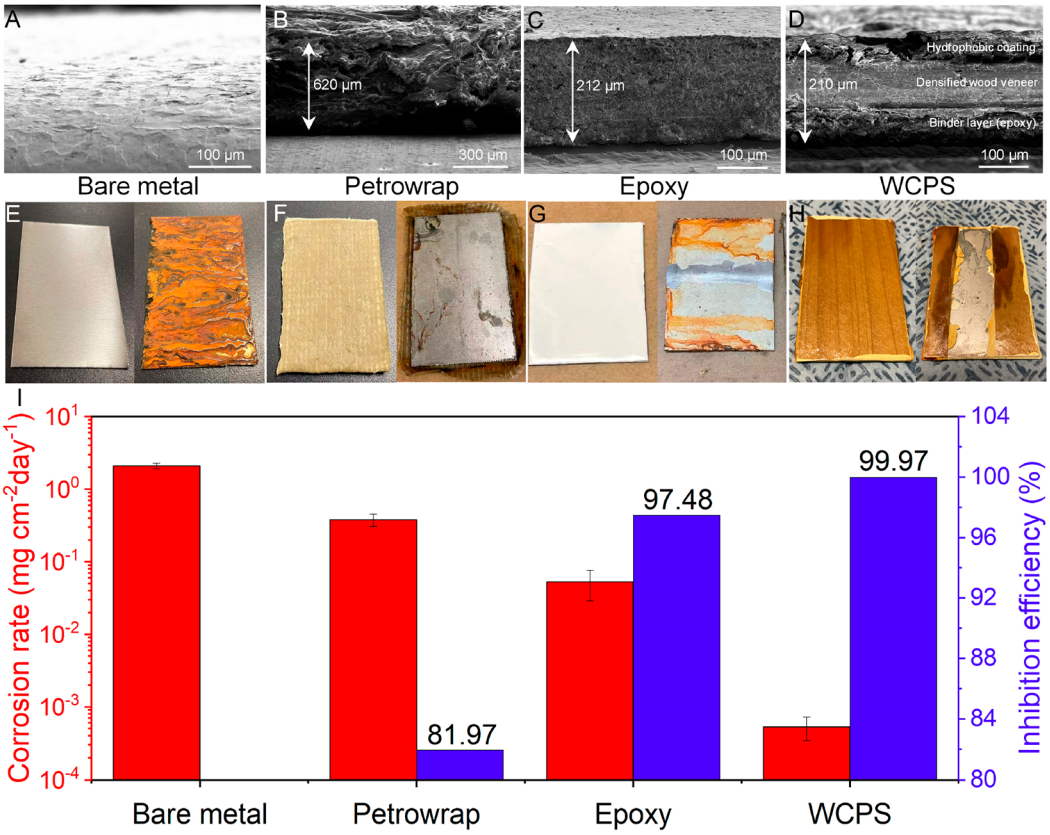

Figure 4. Corrosion performance evaluation of protection layers. SEM images and digital images of (A)(E) bare C-steel plates and C-steel with (B)(F) petrowrap, (C)(G) epoxy, and (D)(H) WCPS before and after the corrosion test, respectively. (I) Corrosion rates and inhibition efficiencies of C-steel plates with various protective layers evaluated by ASTM B117 (720 h) and ASTM G1 (C.3.5.). The error bars describe the distribution of three repeated data points.

diffusion toward the remaining portion of the wood veneer (Movie S6).

Low-rate and selective ion transport in densified wood veneer (without hydrophobic coating) is demonstrated by using concentration-driven dialysis tests combined with inductively coupled plasma mass spectrometry (ICP−MS) (Figure 3A,B and Figure S9). Densified wood veneer shows diffusivities of Cl^-, Na^+, Zn^{2+}, and Fe^{2+} ions down to the order of 10^{-12} m^2 s^{-1}, much lower than those in water (10^{-9} m^2 s^{-1}). For Fe^{3+} and Al^{3+} ions, the diffusivities are reduced to 1×10^{-13} m^2 s^{-1}. The low diffusivity of ions can be explained by the highly dense structure of densified wood as well as the effect of Donnan exclusion. A coin-cell setup is employed to measure the ionic conductivity of NaCl within densified wood veneer (Figure 3C and Figure S10).[41,42] When the concentration of NaCl is lower than 0.1 M, the ionic conductivity is 0.1 mS cm^{-1} regardless of salt concentration, confirming the effect of Donnan exclusion when the ionic conductivity is controlled by the surface charge density of densified wood veneer.[43] Since the zeta potential of densified wood is negative (−18.3 mV in 0.1 M NaCl solution, Figure 3D), the surface of densified wood veneer is occupied by cations (Na^+). When the sizes of such channels are smaller than the Debye length of chloride ions, they will be rejected by the small wood channels (Figure 3E,F). When the concentration of NaCl is greater than 0.1 M, the Debye length of chloride ions becomes too small to be limited by the pore structure. However, the ionic conductivity with densified wood veneer is still 1 order of magnitude lower than that in water. This is because of the highly dense structure of wood (porosity: 9.7%, Figure 3G,H). Regarding the relationship between porosity and ion blocking performance, we conduct a concentration-driven dialysis test with nondensified wood veneers (porosity: 80%), which has the same chemical composition as densified wood veneers. Clearly, the ion blocking function of structures with only a negative zeta potential but high porosity (open porous structure) is limited (Figure S9). Overall, these results confirm that densified wood veneer with negative charge effectively blocks both chloride ions penetrating from the outside (environment) and corrosion products diffusing away from the inside, which is crucial for the performance of corrosion protection.

We evaluate the corrosion protection ability of petrowrap (Figure 4B,F), epoxy (Figure 4C,G), and the WCPS (Figure 4D,H) for low-carbon steel (C-steel, Figure 4A,E) with the ASTM B117 standard protocol (5 wt % NaCl salt spray, 35 °C, 720 h) combined with the ASTM G1 (C.3.5.) standard protocol. After salt spray exposure, the bare C-steel is covered by yellow-brown corrosion products and shows a corrosion rate of 2.09 ± 0.18 mg cm^{-2} day^{-1} (Figure 4E). With SOA protective layers, overall corrosion is highly mitigated except for crevice corrosion near sample edges and in defect-rich regions (Figure 4F,G). The corrosion rates are reduced to 0.05 ± 0.02 mg cm^{-2} day^{-1} (epoxy, inhibition efficiency: 97.48%) and 0.38 ± 0.07 mg cm^{-2} day^{-1} (petrowrap, inhibition efficiency: 81.97%), respectively. With WCPS protection, no obvious corrosion products could be found (Figure 4H). It successfully reduces the corrosion rate of C-steel to ((0.53 ±

https://doi.org/10.1021/acs.nanolett.3c03856
Nano Lett. 2024, 24, 245−253

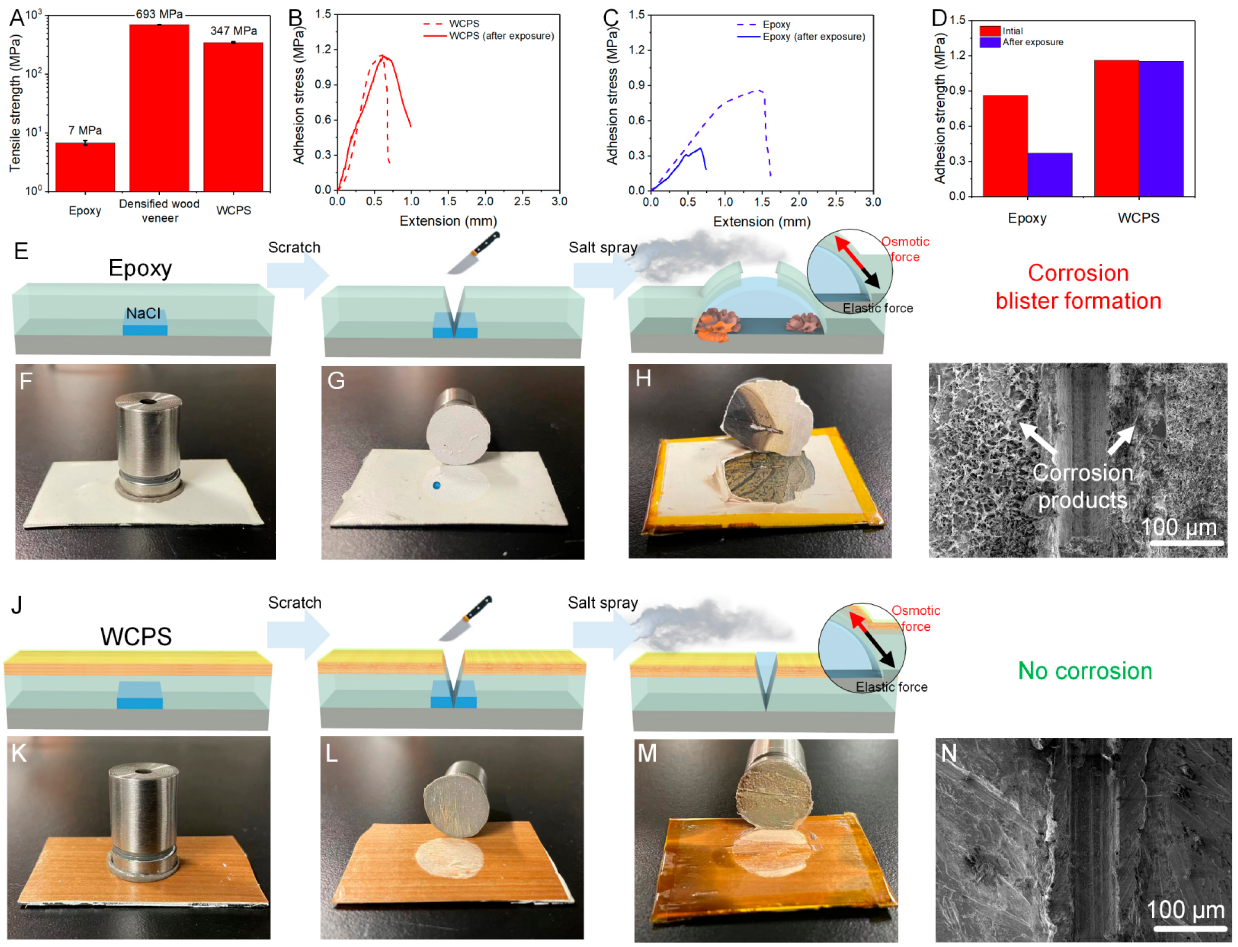

Figure 5. Durability evaluation of corrosion protection layers. (A) Tensile strength of petrowrap, epoxy, and densified wood veneer. (B–D) Adhesive strength as a function of extension during pull-off tests of the WCPS and epoxy. Photographs and schematic illustration of durability evaluation of the (E–I) epoxy and (J–M) WCPS, respectively. SEM characterizations of the metal surface under damaged (I) epoxy and (N) WCPS after exposure (ASTM B117, 240 h), respectively.

0.18) × 10^{-3} mg cm^{-2} day^{-1}, which is 2 orders of magnitude better than epoxy, achieving a high inhibition efficiency of 99.97%. These performance values compare favorably with those of other reported coating structures (Table S2).

Furthermore, we evaluate the corrosion protection ability of protective layers when suffering from physical damage, including chipping (Figure S11), bending (Figure S12), and scribing (Figure S13), also with the ASTM B117 standard protocol. As mentioned above (Figure S4), densified wood veneer shows great damage resistance, whereas epoxy and petrowrap will fail in many mechanical abuse test conditions. The generation of defects compromises the local protective ability of epoxy and petrowrap. In contrast, WCPS offers stable corrosion protection under all test conditions. This evaluation shows that introducing densified wood veneer as an intermediate coat can enhance the structural stability of the whole protective layer and its corrosion protection function under harsh conditions.

The damaged protective layer will lose blocking ability to all corrosive agents, including water, salts, and gases. Small amounts of corrosion products and embedded corrosion inhibitors, often hydrophilic, will attract water from the environment due to osmotic pressure across the protective layer. Densified wood veneer with 2 orders of magnitude higher tensile strength than SOA corrosion protection layers can overcome this blister formation-induced mechanical failure (Figure 5A). A small amount of NaCl (~1 mg) is stored between the metal surface and the protective layer. We then scratch the protective layer to open a 2 cm (length) × 70 μm (width) gap. The sample is then evaluated using the ASTM B117 standard protocol. The pull-off strength in the damaged region is recorded as the adhesive strength. Before salt spray tests, the adhesive strengths of WCPS and epoxy are 1.2 and 0.8 MPa, respectively (Figure 5B). It is worth mentioning that the epoxy layer fails at the epoxy–epoxy interface (Figure 5G) and WCPS fails due to bulk delamination (Figure 5L). After salt spray tests, the epoxy layer fails at the epoxy–metal interface (Figure 5H) with a reduced adhesive strength of 0.4 MPa, and corrosion product can be found near the scratch line (Figure 5I). In contrast, WCPS still fails due to bulk delamination (Figure 5M) with similar adhesive strength, and the corrosion issue is significantly less obvious near the scratch line (Figure 5N). Additionally, with both systems exhibiting a similar strain before delamination (~0.7 mm), we conclude that the interface toughness between the WCPS–metal layers is stronger than that of epoxy–metal. These observations confirm that densified wood veneer as a mechanically strong intermediate layer can dramatically improve the structural stability of the whole protective layer against the blister formation issue, even with physical damage.

https://doi.org/10.1021/acs.nanolett.3c03856
Nano Lett. 2024, 24, 245–253

In this work, we report a thin, mechanically strong, and damage-tolerant densified wood veneer as a core component of a sustainable corrosion protection structure. The mechanical strength overcomes layer delamination caused by blisters formed by swelling of hydrophilic corrosion products due to osmotic pressures across the protection layers. Compared with SOA corrosion protection layers (epoxy and petrowrap), the wood corrosion protection structure can further reduce the corrosion rate of C-steel by 2 orders of magnitude. Meanwhile, the densified wood veneer has several advantages as a sustainable material, with a much lower environmental impact than epoxy and petrowrap. Our work has mainly evaluated the corrosion protection functions of WCPS under salt spray protocols, ASTM B117 (720 h). Further long-term exposure work is needed to consider other conditions, e.g., the effects of wood degradation, fungus, and termites.[44] It is true that the partial delignification reduces the lignin mass percentage (vs the total mass), which could potentially reduce the resiliency of the material to fungal decay. However, the densification process at the same time increases the lignin volume percentage compared with the nondensified counterpart. This enhancement has the potential to improve the fungal resistance of the densified wood veneer. The surface hydrophobic treatment can also improve the stability of densified wood veneer against fungal spores and humidity.

■ ASSOCIATED CONTENT

Supporting Information

The Supporting Information is available free of charge at https://pubs.acs.org/doi/10.1021/acs.nanolett.3c03856.

Chipping test of petrowrap (MP4)

Chipping test of epoxy (MP4)

Chipping test of densified wood (MP4)

Chipping test of WCPS (MP4)

Self-recovery of densified wood (MP4)

Simulated self-recovery of densified wood (MP4)

Materials and methods; notes for finite element modeling (FEM); figures of wood composition analysis, mechanical performance comparison, stress−strain curve, pictures of corrosion protection layers and damage resistance performance, Brinell hardness tests, scribing evaluation of densified wood veneer, influence of salt water on mechanical properties concentration-driven dialysis tests; photos of components of conductivity measurements, chipping-corrosion evaluation, chipping-corrosion evaluation, and scribing-corrosion evaluation; tables of protective layer tensile strengths, summary of advanced corrosion protection structures, mechanical properties of densified wood, and cost of and comprehensive evaluation of epoxy, petrowrap, and WCPS (PDF)

■ AUTHOR INFORMATION

Corresponding Authors

Teng Li − *Department of Mechanical Engineering, University of Maryland, College Park, Maryland 20742, United States;* orcid.org/0000-0001-6252-561X; Email: lit@umd.edu

Liangbing Hu − *Department of Materials Science and Engineering, University of Maryland, College Park, Maryland 20742, United States;* orcid.org/0000-0002-9456-9315; Email: binghu@umd.edu

Ping Liu − *Program of Materials Science, University of California San Diego, La Jolla, California 92093, United States; Department of NanoEngineering and Chemical Engineering and Program of Chemical Engineering, University of California San Diego, La Jolla, California 92093, United States;* orcid.org/0000-0002-1488-1668; Email: piliu@ucsd.edu

Authors

Sicen Yu − *Program of Materials Science, University of California San Diego, La Jolla, California 92093, United States*

Yu Liu − *Department of Materials Science and Engineering, University of Maryland, College Park, Maryland 20742, United States*

Qiongyu Chen − *Department of Mechanical Engineering, University of Maryland, College Park, Maryland 20742, United States;* orcid.org/0000-0001-5283-5614

Xiaolu Yu − *Program of Materials Science, University of California San Diego, La Jolla, California 92093, United States*

Gayea Hyun − *Department of NanoEngineering and Chemical Engineering, University of California San Diego, La Jolla, California 92093, United States*

Shen Wang − *Department of NanoEngineering and Chemical Engineering, University of California San Diego, La Jolla, California 92093, United States;* orcid.org/0000-0003-3826-4397

Yuhang Ye − *Department of Wood Science, University of British Columbia, Vancouver, BC V6T 1Z4, Canada*

Jiaqi Feng − *Program of Chemical Engineering, University of California San Diego, La Jolla, California 92093, United States*

Zheng Chen − *Program of Materials Science, University of California San Diego, La Jolla, California 92093, United States; Department of NanoEngineering and Chemical Engineering and Program of Chemical Engineering, University of California San Diego, La Jolla, California 92093, United States;* orcid.org/0000-0002-9186-4298

Feng Jiang − *Department of Wood Science, University of British Columbia, Vancouver, BC V6T 1Z4, Canada;* orcid.org/0000-0003-2497-9922

Joseph King − *Advanced Research Projects Agency - Energy, U.S. Department of Energy, Washington, D.C. 20585, United States*

Complete contact information is available at: https://pubs.acs.org/10.1021/acs.nanolett.3c03856

Author Contributions

S.Y. and Y.L. contributed equally to this work. P.L. and L.H. supervised the project. S.Y., P.L., and L.H. designed the experiments. S.Y. carried out corrosion evaluation and the data analysis. Y.L. carried out the wood preparation and composition analysis. Q.C. and T.L. carried out FEM modeling. X.Y. and Z.C. carried out ICP tests. S.W. carried out cryo-FIB. Y.Y. and F.J. measured zeta potential of wood samples. G.H. and J.F. designed and drew schematic diagrams. J.K. proposed the effect of temperature on self-recovery performance of wood. All authors contributed to the writing of the manuscript. All authors commented on the final manuscript.

Notes

The authors declare no competing financial interest.

https://doi.org/10.1021/acs.nanolett.3c03856
Nano Lett. 2024, 24, 245−253

■ ACKNOWLEDGMENTS

We acknowledge the support from the University of California at San Diego and its Center for Memory and Recording Research (CMRR), the support from the University of Maryland A. James Clark School of Engineering, the University of Maryland supercomputing resources (https://hpcc.umd.edu), and Maryland Advanced Research Computing Center (MARCC) for conducting the research reported in this work. This work is performed in part at the San Diego Nanotechnology Infrastructure (SDNI) of University of California San Diego, a member of the National Nanotechnology Coordinated Infrastructure (NNCI), which is supported by the National Science Foundation (Grant ECCS-1542148). This work is supported by the Advanced Research Projects Agency-Energy (ARPA-E) of the U.S. Department of Energy under Contract no. DE-FOA-0001858 to L.H., T.L., and P.L.

■ REFERENCES

(1) Strivens, T.; Lambourne, R. *Paint and surface coatings: theory and practice*; Woodhead, 1999.
(2) Sidky, P.; Hocking, M. Review of inorganic coatings and coating processes for reducing wear and corrosion. *British Corrosion Journal* **1999**, *34* (3), 171−183.
(3) Zayat, M.; Garcia-Parejo, P.; Levy, D. Preventing UV-light damage of light sensitive materials using a highly protective UV-absorbing coating. *Chem. Soc. Rev.* **2007**, *36* (8), 1270−1281.
(4) Zhou, H.; Yu, S.; Liu, H.; Liu, P. Protective coatings for lithium metal anodes: Recent progress and future perspectives. *J. Power Sources* **2020**, *450*, No. 227632.
(5) Salam Hamdy, A.; Butt, D. P. Corrosion protection performance of nano-particles thin-films containing vanadium ions formed on aluminium alloys. *Anti-Corrosion Methods and Materials* **2006**, *53* (4), 240−245.
(6) Holm, E.; Transeth, A. A.; Knudsen, O. Ø.; Stahl, A. *Classification of corrosion and coating damages on bridge constructions from images using convolutional neural networks*; Twelfth International Conference on Machine Vision (ICMV 2019); International Society for Optics and Photonics, 2020; p 1143320.
(7) Larsson, M.; Olsson, M.; Hedenqvist, P.; Hogmark, S. Mechanisms of coating failure as demonstrated by scratch and indentation testing of TiN coated HSS. *Surface engineering* **2000**, *16* (5), 436−444.
(8) Effendy, S.; Zhou, T.; Eichman, H.; Petr, M.; Bazant, M. Z. Blistering failure of elastic coatings with applications to corrosion resistance. *Soft Matter* **2021**, *17* (41), 9480−9498.
(9) Liu, B.-s.; Wei, Y.-h.; Chen, W.-y.; Hou, L.-f.; Guo, C.-l. Blistering failure analysis of organic coatings on AZ91D Mg-alloy components. *Engineering Failure Analysis* **2014**, *42*, 231−239.
(10) Utrera-Barrios, S.; Verdejo, R.; López-Manchado, M. A.; Santana, M. H. Evolution of self-healing elastomers, from extrinsic to combined intrinsic mechanisms: A review. *Materials Horizons* **2020**, *7* (11), 2882−2902.
(11) Zhang, F.; Ju, P.; Pan, M.; Zhang, D.; Huang, Y.; Li, G.; Li, X. Self-healing mechanisms in smart protective coatings: A review. *Corros. Sci.* **2018**, *144*, 74−88.
(12) Zadeh, M. A.; Van Der Zwaag, S.; Garcia, S. Routes to extrinsic and intrinsic self-healing corrosion protective sol-gel coatings: a review. *Self-Heal. Mater.* **2013**, *1*, 1−18.
(13) Chang, K.; Jia, H.; Gu, S.-Y. A transparent, highly stretchable, self-healing polyurethane based on disulfide bonds. *Eur. Polym. J.* **2019**, *112*, 822−831.
(14) Cho, S. H.; White, S. R.; Braun, P. V. Self-healing polymer coatings. *Adv. Mater.* **2009**, *21* (6), 645−649.
(15) Nesterova, T.; Dam-Johansen, K.; Pedersen, L. T.; Kiil, S. Microcapsule-based self-healing anticorrosive coatings: Capsule size, coating formulation, and exposure testing. *Prog. Org. Coat.* **2012**, *75* (4), 309−318.
(16) Calvino, C.; Weder, C. Microcapsule-Containing Self-Reporting Polymers. *Small* **2018**, *14* (46), No. 1802489.
(17) Bertrand, G.; Mahdjoub, H.; Meunier, C. A study of the corrosion behaviour and protective quality of sputtered chromium nitride coatings. *Surf. Coat. Technol.* **2000**, *126* (2−3), 199−209.
(18) Kendig, M.; Jeanjaquet, S.; Addison, R.; Waldrop, J. Role of hexavalent chromium in the inhibition of corrosion of aluminum alloys. *Surf. Coat. Technol.* **2001**, *140* (1), 58−66.
(19) Schem, M.; Schmidt, T.; Caparrotti, H.; Wittmar, M.; Veith, M. Corrosion inhibiting cerium compounds for chromium-free corrosion protective coatings on AA 2024. *Self-healing properties of new surface treatments EFC* **2011**, *58*, 184.
(20) Liu, X.; Zhang, H.; Wang, J.; Wang, Z.; Wang, S. Preparation of epoxy microcapsule based self-healing coatings and their behavior. *Surf. Coat. Technol.* **2012**, *206* (23), 4976−4980.
(21) Yang, C.; Xu, W.; Meng, X.; Shi, X.; Shao, L.; Zeng, X.; Yang, Z.; Li, S.; Liu, Y.; Xia, X. A pH-responsive hydrophilic controlled release system based on ZIF-8 for self-healing anticorrosion application. *Chemical Engineering Journal* **2021**, *415*, No. 128985.
(22) Camilli, L.; Yu, F.; Cassidy, A.; Hornekær, L.; Bøggild, P. Challenges for continuous graphene as a corrosion barrier. *2D Materials* **2019**, *6* (2), No. 022002.
(23) Al-Sahari, A.; Toor, I. U.-H. Rehabilitation coatings-current challenges and opportunities for the future. *Liquid and Gaseous Energy Resources* **2022**, *2* (1), 1−14.
(24) Wang, H.; Xu, J.; Du, X.; Du, Z.; Cheng, X.; Wang, H. A self-healing polyurethane-based composite coating with high strength and anti-corrosion properties for metal protection. *Composites Part B: Engineering* **2021**, *225*, No. 109273.
(25) Wang, X.; Tang, F.; Cao, Q.; Qi, X.; Pan, H.; Chen, X.; Lin, Z. Carbon-Based Nanoparticle-Filled Protective Coatings for Enhanced Damage Tolerance and Corrosion Resistance of Structural Weldment. *Journal of Materials in Civil Engineering* **2022**, *34* (1), No. 04021384.
(26) Enos, D.; Guilbert, C.; Kehr, J. A. *Improving the damage tolerance, and extending the service life of fusion-bonded epoxy coatings*; CORROSION 2001; OnePetro, 2001.
(27) Chuang, T.-J.; Nguyen, T.; Lee, S. Micro-mechanic model for cathodic blister growth in painted steel. *Journal of Coatings Technology* **1999**, *71* (895), 75−85.
(28) Domun, N.; Hadavinia, H.; Zhang, T.; Sainsbury, T.; Liaghat, G.; Vahid, S. Improving the fracture toughness and the strength of epoxy using nanomaterials−a review of the current status. *Nanoscale* **2015**, *7* (23), 10294−10329.
(29) Somarathna, H.; Raman, S.; Mohotti, D.; Mutalib, A.; Badri, K. The use of polyurethane for structural and infrastructural engineering applications: A state-of-the-art review. *Construction and Building Materials* **2018**, *190*, 995−1014.
(30) Pistone, A.; Scolaro, C.; Visco, A. Mechanical properties of protective coatings against marine fouling: A review. *Polymers* **2021**, *13* (2), 173.
(31) Song, J.; Chen, C.; Zhu, S.; Zhu, M.; Dai, J.; Ray, U.; Li, Y.; Kuang, Y.; Li, Y.; Quispe, N. Processing bulk natural wood into a high-performance structural material. *Nature* **2018**, *554* (7691), 224−228.
(32) Chen, C.; Kuang, Y.; Zhu, S.; Burgert, I.; Keplinger, T.; Gong, A.; Li, T.; Berglund, L.; Eichhorn, S. J.; Hu, L. Structure−property−function relationships of natural and engineered wood. *Nature Reviews Materials* **2020**, *5* (9), 642−666.
(33) Yu, S.; Liu, Y.; Chen, C.; Feng, S.; Siciliano, A. P.; Hu, L.; Liu, P. A low-corrosivity structural timber. *Cell Reports Physical Science* **2022**, *3* (6), No. 100921.
(34) Dong, X.; Gan, W.; Shang, Y.; Tang, J.; Wang, Y.; Cao, Z.; Xie, Y.; Liu, J.; Bai, L.; Li, J. Low-value wood for sustainable high-performance structural materials. *Nature Sustainability* **2022**, *5* (7), 628−635.
(35) Chen, W.; Bu, Y.; Li, D.; Liu, C.; Chen, G.; Wan, X.; Li, N. High-strength, tough, and self-healing hydrogel based on carboxymethyl cellulose. *Cellulose* **2020**, *27*, 853−865.

https://doi.org/10.1021/acs.nanolett.3c03856
Nano Lett. 2024, 24, 245−253

(36) Santos, D.; Brites, C.; Costa, M.; Santos, M. Performance of paint systems with polyurethane topcoats, proposed for atmospheres with very high corrosivity category. *Prog. Org. Coat.* **2005**, *54* (4), 344−352.
(37) Afshar, A.; Jahandari, S.; Rasekh, H.; Shariati, M.; Afshar, A.; Shokrgozar, A. Corrosion resistance evaluation of rebars with various primers and coatings in concrete modified with different additives. *Construction and Building Materials* **2020**, *262*, No. 120034.
(38) Momber, A.; Plagemann, P.; Stenzel, V. Performance and integrity of protective coating systems for offshore wind power structures after three years under offshore site conditions. *Renewable Energy* **2015**, *74*, 606−617.
(39) Schremp, F. Corrosion prevention for offshore platforms. *Journal of petroleum technology* **1984**, *36* (04), 605−612.
(40) Beverly, S.; SPC, N. Fisheries Development Officer visits Fish Expo in Seattle, Washington, USA. *FISHERIES NEWSLETTER-SOUTH PACIFIC COMMISSION* **2000**, 31−35.
(41) Tan, R.; Wang, A.; Malpass-Evans, R.; Williams, R.; Zhao, E. W.; Liu, T.; Ye, C.; Zhou, X.; Darwich, B. P.; Fan, Z. Hydrophilic microporous membranes for selective ion separation and flow-battery energy storage. *Nat. Mater.* **2020**, *19* (2), 195−202.
(42) Li, T.; Li, S. X.; Kong, W.; Chen, C.; Hitz, E.; Jia, C.; Dai, J.; Zhang, X.; Briber, R.; Siwy, Z. A nanofluidic ion regulation membrane with aligned cellulose nanofibers. *Science advances* **2019**, *5* (2), No. eaau4238.
(43) Li, S. X.; Guan, W.; Weiner, B.; Reed, M. A. Direct observation of charge inversion in divalent nanofluidic devices. *Nano Lett.* **2015**, *15* (8), 5046−5051.
(44) Ding, Y.; Pang, Z.; Lan, K.; Yao, Y.; Panzarasa, G.; Xu, L.; Lo Ricco, M.; Rammer, D. R.; Zhu, J.; Hu, M. Emerging engineered wood for building applications. *Chem. Rev.* **2023**, *123* (5), 1843−1888.

https://doi.org/10.1021/acs.nanolett.3c03856
Nano Lett. 2024, 24, 245−253